THE JOURNAL OF PHYSICAL CHEMISTRY C

Article

pubs.acs.org/JPCC

Surface Structure, Morphology, and Stability of $Li(Ni_{1/3}Mn_{1/3}Co_{1/3})O_2$ Cathode Material

Juan C. Garcia,[†] Javier Bareño,[‡] Jianhua Yan,[§] Guoying Chen,[§] Andrew Hauser,[∥] Jason R. Croy,[‡] and Hakim Iddir*[,†]

[†]Materials Science Division, Argonne National Laboratory, Argonne, Illinois 60439, United States

[‡]Chemical Sciences and Engineering Division, Argonne National Laboratory, Argonne, Illinois 60439, United States

[§]Energy Storage and Distributed Resources Division, Lawrence Berkeley National Laboratory, Berkeley, California 94720, United States

[∥]University of Wisconsin-Madison, Madison, Wisconsin 53706-1390, United States

ABSTRACT: Layered $Li(Ni_{1-x-y}Mn_xCo_y)O_2$ (NMC) oxides are promising cathode materials capable of addressing some of the challenges associated with next-generation energy storage devices. In particular, improved energy densities, longer cycle-life, and improved safety characteristics with respect to current technologies are needed. However, sufficient knowledge on the atomic-scale processes governing these metrics in working cells is still lacking. Herein, density functional theory (DFT) is employed to predict the stability of several low-index surfaces of $Li(Ni_{1/3}Mn_{1/3}Co_{1/3})O_2$ (NMC111) as a function of Li and O chemical potentials. Predicted particle shapes are compared with those of single crystal NMCs synthesized under different conditions. The most stable surfaces for stoichiometric NMC111 are predicted to be the nonpolar (104), the polar (012) and (001), and the reconstructed, polar (110) surfaces. Results indicate that intermediate spin Co^{3+} ions lower the (104) surface energy. Furthermore, it was found that removing oxygen from the (012) surface was easier than from the (104) surface, suggesting a facet dependence on surface-oxygen vacancy formation. These results give important insights into design criteria for the rational control of synthesis parameters as well as establish a foundation on which future mechanistic studies of NMC surface instabilities can be developed.

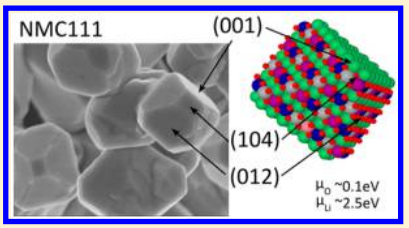

1. INTRODUCTION

Energy storage devices with high energy densities are needed in order to meet the increasing demands of portable electronics and electric vehicles. Layered $Li(Ni_{1-x-y}Mn_xCo_y)O_2$ (NMC) oxides are promising cathode materials that are intrinsically capable of meeting many of these demands.[1−3] However, in order to take advantage of these high, intrinsic energies, charging voltages of >4.2 V (vs graphite) are necessary. At such high voltages, surface degradation phenomena take place at untenable rates, thereby reducing the battery lifetime. Therefore, to take full advantage of NMC-based, lithium-ion cells, the fundamental processes underlying issues of surface reactivity must be fully understood. Toward this end, it is a prerequisite to determine an atomic-scale view of the most relevant NMC surfaces at play. Only after this can a mechanistic understanding of NMC surface-reactivity be developed.

Layered $LiCoO_2$ (LCO) has been successfully used for years as a cathode material. However, because of LCO's low intrinsic stability at high states of charge (SOC), it is limited in practical capacity. Large-scale substitution of Co with different transition metals (TMs), (i.e., Mn and Ni to create NMCs) has been shown to improve stability at higher SOCs; promising both higher energy densities and lower costs with respect to pure LCO.[4−6] The structure of these layered materials (space group $R\bar{3}m$) can be interpreted as an ordered rocksalt with alternate layers of lithium and metal ions occupying octahedral sites in a cubic close-packed oxygen array with an ABCABC stacking sequence.[7] This structure facilitates the relatively facile removal of Li^+ ions, where the practical capacity of layered materials depends on the range of concentrations, x in $Li_{1-x}MO_2$ (M = Mn, Ni, Co), over which Li^+ ions can be reversibly intercalated.[8,9] Key to this reversibility is the ratio of Mn:Ni:Co. In particular, Li:Ni antisite exchange between the layers, mitigated by the presence of Co, can have a profound effect. In addition, irreversible surface reconstructions have been reported to affect cell performance via impedance rise and capacity loss. The nature of reconstructed surfaces may play an important role in understanding chemical interactions with electrolytes.[10−14] Experimental data,[15] as well as our own AIMD simulations (not included here), suggest that surface reactivity plays a key role in cell degradation before the onset of bulk instabilities. As such, the most pressing challenges to the practical, high-energy implementation of NMC cathodes are phenomena related to surface instabilities, electrode-crosstalk, and capacity fade when cells are cycled to the necessary cutoff voltages (>4.2 V vs graphite).[16,17]

Knowledge of the nature and proportion of the different facets of NMC crystals can help in the understanding of

Received: January 27, 2017
Revised: March 17, 2017
Published: March 28, 2017

DOI: 10.1021/acs.jpcc.7b00896
J. Phys. Chem. C XXXX, XXX, XXX−XXX

interfacial phenomena. For example, the rate performance of batteries has a dependence on the characteristics of the particle surfaces and orientation, which controls the kinetics of Li diffusion and the stability of the surface phase transitions. Different factors such as chemical composition, crystal structure, and different morphologies can also produce various interface structures and crystal surfaces.[18] A DFT study on the structure of LCO found that the (104), (001), and (012) surfaces are present in the equilibrium crystal shape.[19] The same study also found that the (104) surface has the highest stability among the nonpolar surfaces, in agreement with experimental findings.[20,21] Another theoretical study found the same facets to be the most stable surfaces for $LiNiO_2$. However, the surface energies of $LiNiO_2$ were smaller than those of LCO for all facets.[22] The unit cell volume of NMC111 (100.6 Å^3) is midway between LCO (96.8 Å^3) and $LiNiO_2$ (102.3 Å^3).[4] To the best of our knowledge, comprehensive theoretical studies to determine NMC particle morphologies, surface energies, and surface terminations have not been conducted. In the present work, we use density functional theory (DFT) to identify the lowest energy surfaces of low-index facets of NMC111. The Wulff construction[23] is used to predict the thermodynamic equilibrium particle shape as a function of O and Li surface coverage. The results are compared with experimentally observed particle shapes of single-crystal NMCs, synthesized under various conditions and, as shown, may be extended, in general, to other NMC compositions.

2. METHODOLOGY

All calculations were carried out by spin-polarized DFT as implemented in the Vienna Ab Initio Simulation Package (VASP).[24,25] The exchange-correlation potentials are treated by the generalized gradient approximation (GGA) parametrized by Perdew, Burke, and Ernzerholf (PBE).[26] The interaction between valence electrons and ion cores is described by the projected augmented wave (PAW) method.[27] Furthermore, the GGA+U scheme is used for applying the on-site correlation effects among 3d electrons of the TM, where the parameter of (U−J) is set to 5.96, 5.00, and 4.84 eV for Ni, Co, and Mn, respectively.[28] The wave functions were expanded in the plane wave basis up to a kinetic energy of 500 eV. All surface calculations were performed using a periodically repeating slab separated by vacuum layers along the surface normal. A vacuum thickness of 10 Å was adopted to remove interaction between the slab layers. The lattice parameter of the supercell was fixed at its bulk value. All the ions were allowed to be relaxed until the total energy differences were no more than 0.003 eV. After geometry optimization within the DFT+U framework, electronic relaxation was performed using a single point calculation with the hybrid functional HSE06,[29] to determine the surface energy at that level of theory. Figure 1a shows the bulk crystal structure of NMC111 ($R\bar{3}m$). In order to establish the ion ordering in the TM layers, it is necessary to use a supercell that is at least three times bigger in the a and b directions than for a single-metal, layered material such as $LiCoO_2$. A k-point mesh of 3 × 3 × 3 was found sufficient to get accurate electronic energies for bulk calculations on this unit cell. The resultant ion ordering is shown in Figure 1b. Each ion has six neighbors in groups of three of the other TM arranged in a triangular shape. This ordering has been found to be the most favorable using solid state NMR.[30] This structure was also confirmed by DFT calculations of an initial set of 30 lowest energy configurations determined based on electrostatic

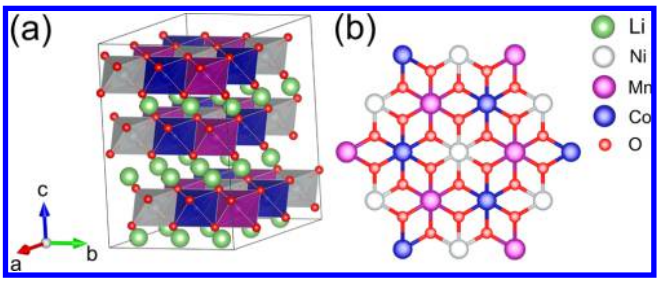

Figure 1. Illustration of the bulk geometry of NMC111 with $R\bar{3}m$ symmetry. (b) Schematic representation of ion-ordering in NMC111 TM layers.

interactions only (not shown). The ordering can be explained based on the local charge balance. The sum of the electrovalencies of the nearest-neighbor cations should be equal to the charge of the anion in ordered rocksalt structures.

All low index families of surfaces were considered; limited herein to stoichiometric surfaces. That is, unit cells consist of an integer number of formula units. Among the surfaces considered, some are polar surfaces. As a consequence, it is necessary to cancel the total dipole of the slab in order to get meaningful results within the DFT periodic boundary conditions approach. Charge compensation was accomplished by moving half of the charge from the top layer to the bottom layer.

2.1. (110) Surface. An index notation based on the original standard hexagonal unit cell was used. The polar surfaces examined were the (110), (012), and (001). In order to illustrate the procedure used to avoid a dipole in the slabs, we consider the (110) surface as an example. A schematic diagram of the slab representing the (110) surface is shown in Figure 2a. We can consider the slab as a stack of layers. The layers parallel to the surface contain two kinds of TM ions, a consequence of the ordering and stacking that we chose for the TM. This ordering produces a configuration with two kinds of layers having a total formal charge of +1 and −2. This configuration leads to a surface type III according to the classification proposed by Tasker.[31] A polar surface cannot be stable without substantial reconstruction. Figure 2b shows a possible rearrangement of the TM ions that produces a Tasker type I surface, that is all the layers are neutral. This configuration is possible because each layer maintains a stoichiometric ratio of atoms. To form this configuration from the original slab, the TMs on one layer are displaced one position up in the direction perpendicular to the surface. The positions of the ions are the same as in the original slab. However, the nature of the ions has changed. Now, there is one TM of each type per unit cell in all the layers. Hence, each layer has a stoichiometric ratio of the species. The shifting of a complete TM with respect to the other layers is in fact an extended defect that does not seem to considerably affect the total energy of the bulk structure (ΔE = 0.02 eV). This "reconstruction" is in fact a bulk transformation rather than a surface reconstruction, as it requires a new stacking sequence of the TM layers. Hence, a different reconstruction is needed to eliminate the overall dipole of the (110) slab.

A more natural reconstruction of the original (110) surface slab, with the constraint of keeping the slab stoichiometric, is obtained by moving half of the surface atoms (hence charge) from the top layer to the bottom of the slab, converting the surface to a Tasker type II. A symmetry plane is created in the

DOI: 10.1021/acs.jpcc.7b00896
J. Phys. Chem. C XXXX, XXX, XXX−XXX

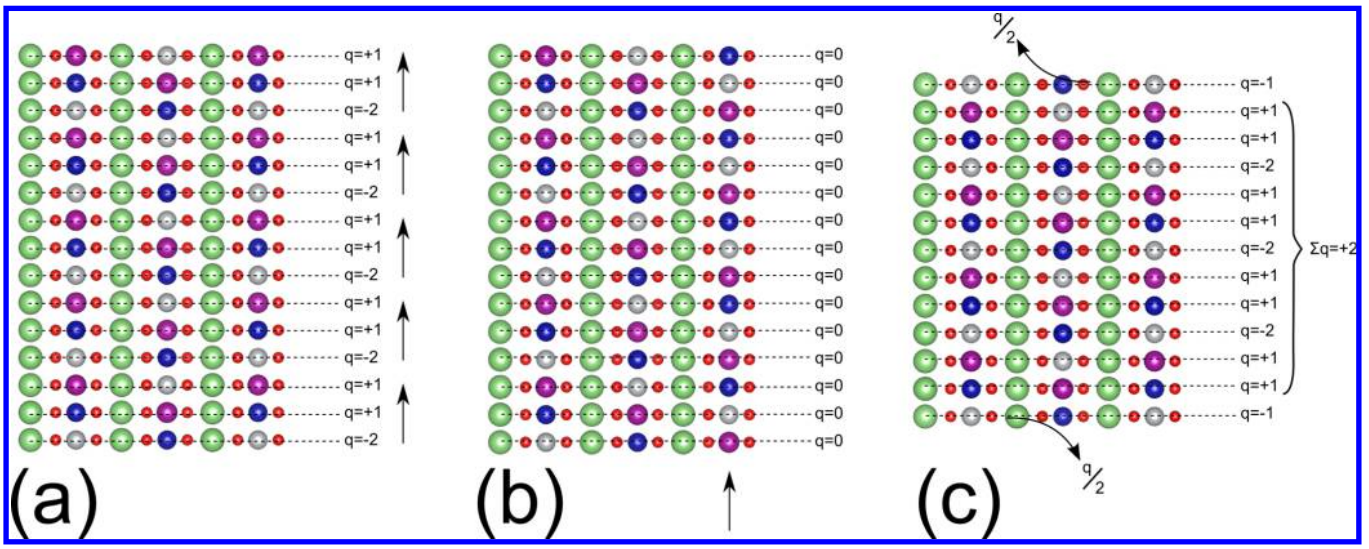

Figure 2. Surface termination and reconstructions for the surface (110). (a) Original slab presenting a finite net dipole. (b) Modified slab where TMs in one of the layers are displaced one position up. (c) Modified slab where half of the charge is taken for the top and bottom layers. Green spheres represent Li, purple spheres represent Mn, gray spheres represent Ni, blue spheres represent Co, and red spheres represent oxygen. The same color scheme is used in the remaining figures.

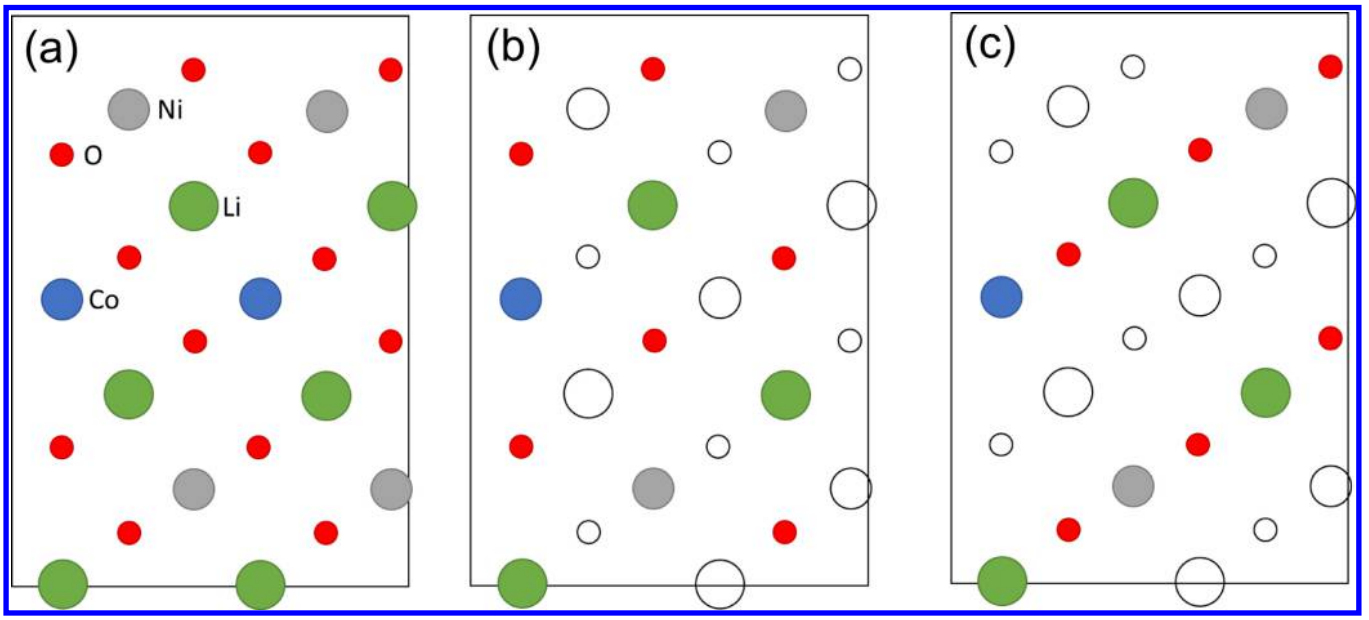

Figure 3. Scheme of the top layer of the surface (110). (a) Original surface with all the ions. (b) Reconstruction where the TMs and Li ions were taken off in rows alternating with rows where oxygen vacancies are formed. (c) Reconstruction where all the TMs, lithium ions, and oxygen ions are taken off from the same row (missing-row reconstruction). Empty circles represent vacancies.

center of the slab and the overall dipole is eliminated. This concept is illustrated in Figure 2c. There are several different ways of ordering the remaining half-coverage atoms on the surface. Figure 3a shows the top layer of the original (110) surface. Figure 3b,c shows the two lowest energy configurations of the surface atoms at half coverage. The surface energy of the configuration shown in Figure 3c is 0.44 eV lower than that in Figure 3b.

2.2. (001) Surface. Another polar surface studied is the (001). This surface can be terminated in different planes. Namely, half a monolayer of lithium on both sides of the slab, lithium deficient 1/2Li−(O−TM−O)−1/2Li layer or oxygen deficient 1/2O−(Li−O−TM)−O1/2 layers. Previous work found that the termination with half a monolayer of Li is more thermodynamically favorable.[19] Therefore, we limit our investigation to this termination. Figure 4 shows a schematic of the slab used for the calculation and the reconstruction of the top and bottom layers. The (001) surface terminated at lithium ions is only sensitive to changes in the chemical potential of lithium. The changes in the Li potential depend on the Li content during material synthesis and on the voltage during cycling.

2.3. (012) Surface. The (012) surface is polar and preferentially terminated by oxygen atoms. A schematic representation of a top view of this configuration is presented in Figure 5. The removal of half of the oxygen atoms from the surfaces compensates the dipoles in the slab. There are two kinds of surface oxygen sites. In site (A), O is coordinated to

DOI: 10.1021/acs.jpcc.7b00896
J. Phys. Chem. C XXXX, XXX, XXX−XXX

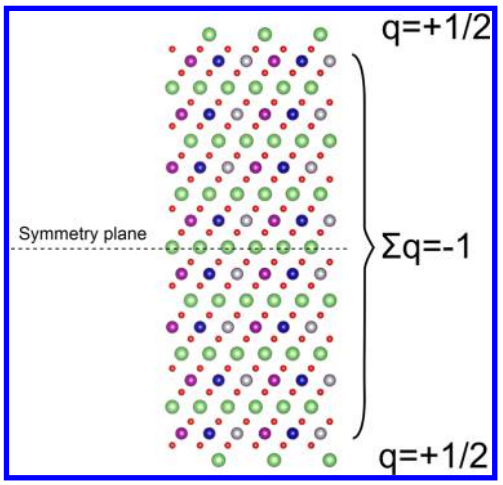

Figure 4. Schematic representation of the slab used to model the (001) surface.

two TM atoms and one lithium atom. In site (B), O is coordinated to two lithium atoms and one TM atom. As expected, and according to previous work,[19] the most stable surface is produced by a configuration where every site A is occupied by an oxygen atom.

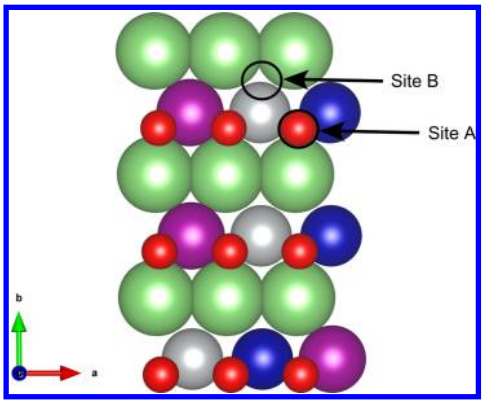

Figure 5. Schematic of the (012) surface with 1/2 monolayer of oxygen coverage. The occupied sites are coordinated with two TMs and one Li-ion (site A). The less favorable site B is also indicated by an empty circle.

We have also considered the nonpolar surfaces (104) and (100). Both of these surfaces are Tasker type I with a stoichiometric ratio of atoms in each layer. Hence, there is no driving force for reconstruction or dependence on O or Li chemical potentials of these surfaces.

The surface energy can be defined as the difference in the free energy between the bulk material and a model slab surface per unit area. For a stoichiometric composition, the surface energy can be computed using eq 1. We also assume the entropic and volumetric contributions to be negligible.

$$\gamma = \frac{1}{2A}(E_{\text{slab}} - E_{\text{bulk}}) \quad (1)$$

where γ is the surface energy, A is the surface area of the slab model, E_{bulk} is the total electronic energy of the bulk material, and E_{slab} is the total electronic energy of the slab. For nonstoichiometric surfaces, the energy of the surface depends on the chemical potential μ_i of the species in excess or shortage (Δ_i). This can be computed according to eq 2

$$\gamma = \frac{1}{2A}(E_{\text{slab}} - E_{\text{bulk}} + \sum_i \Delta_i \mu_i) \quad (2)$$

Experimentally, NMC crystals were synthesized by a molten-salt method previously reported.[14] All chemicals were obtained from Sigma-Aldrich with a purity of 97% or higher. Stoichiometric amounts of $Mn(NO_3)_2{\cdot}4H_2O$, $Co(NO_3)_2{\cdot}6H_2O$, and $Ni(NO_3)_2{\cdot}6H_2O$ were first dissolved in a small amount of deionized water. $LiNO_3$ or Li_2CO_3 in 10% excess (or Li:M = 1.1:1 where M = Mn + Ni + Co) was added to the solution followed by the addition of the CsCl flux (m.p. = 645 °C). The R ratio, defined as the molar ratio between the flux and the total TM, was controlled at 2 or 4. The mixture was transferred into an alumina crucible with a lid, and the trace water was removed by heating to 200 °C at 2 °C/min and then held at 200 °C for 5 h. The resulting dry powder was further heated to 850 or 900 °C at a rate of 4 °C/min, soaked at high temperature for 8 or 12 h, and then cooled to room temperature at a rate of 4 °C/min. The final product was obtained after thoroughly washing with deionized water to remove the flux and then drying in a vacuum oven overnight at 80 °C.

3. RESULTS AND DISCUSSION

3.1. Surface Energies and Morphology. The results of surface energy calculations for stoichiometric slabs are summarized in Table 1. The surface energy is an indication of the relative stability of different facets and terminations. The (104) surface is found to be the lowest surface energy among all the investigated surfaces, as it requires the least amount of bond breaking (one M−O bond). As in previous work[19,32] the trend on surface energy can be rationalized by counting the broken bonds when the surface is cleaved. This surface is nonpolar and each layer contains a stoichiometric amount of each component, making it less sensitive to changes in the O and Li chemical potentials. The flat, nonpolar structure helps stabilize this facet. Figure 6 shows a schematic representation of the (104) surface.

Table 1. Surface Energies for the Low Miller Index Families of Surfaces for NMC111 Under a Stoichiometric Ratio of the Species

surface orientation	surface termination	surface energy (J/m^2)
(104)	Ni, Mn, Co, O	0.76
(001)	Ni, Mn, Co, O	0.89
$(110)_A$[a]	Ni, Mn, Co, O	1.32
$(110)_B$[a]	Co, O	1.67
	Ni, O	1.77
	Mn, O	1.88
(012)	Ni, Mn, Co, O	1.97
(100)	Ni, Mn, Co, O	2.27

[a]$(110)_A$: surface reconstruction. $(110)_B$: bulk extended defect.

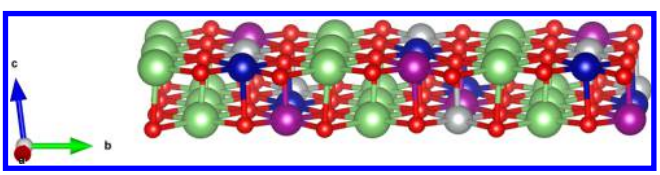

Figure 6. Schematic representation of the top two layers of the (104) surface.

DOI: 10.1021/acs.jpcc.7b00896
J. Phys. Chem. C XXXX, XXX, XXX−XXX

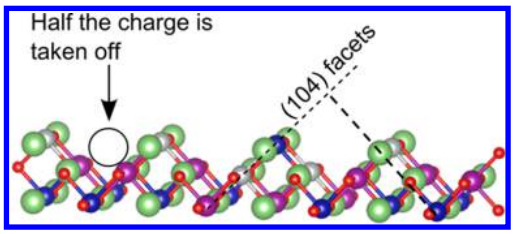

Figure 7. Reconstruction of the (110) surface that leads to lower surface energy. Sites where the ions were taken off are indicated by an empty circle. Also, the (104) facets formed by the reconstructions are indicated by a dashed line.

The (001) surface is the second most stable (see Table 1). In the next section, the sensitivity of the (001) surface to changes in the Li chemical potential is studied. The third most stable surface is the reconstructed (110) surface (a missing-row reconstruction). The TM shifting approach $(110)_B$ (Figure 2b) does not seem to be favorable.

Figure 7 shows a schematic representation of $(110)_A$ reconstructed surface. In this rearrangement, the surface forms a zigzag of (104) facets, such that the surface TMs are also 5-fold coordinated.

The (012) surface is another polar facet considered (see Figure 8a,b). This surface consists of alternating planes of cations and oxygen ions. Thus, there are two possible terminations for a dipole-free model of the slab; either a partially unoccupied, cation-terminated layer, or a partially oxygen-terminated surface. The cation-terminated surface is found to be unstable;[19] hence, an oxygen-terminated surface is studied. The stoichiometric ratio is achieved with half a monolayer of oxygen on the surface. For stoichiometric slabs, the (012) surface is less stable than the (001) surface. However, the partial coverage of oxygen makes the (012) surface sensitive to changes in the oxygen chemical potential. A thermodynamic analysis is needed to estimate the surface energy for different conditions.

Finally, the nonpolar (100) surface presents the highest energy among all the computed surfaces with a surface energy more than double the energy of the other nonpolar, (104) surface. The TMs in the top layer are 3-fold coordinated. This produces a metal−oxygen coordination loss of three compared to one for the (104) surface. Figure 8c shows a schematic representation of this surface.

According to the magnetization and Bader charge analysis, Co^{3+}, Ni^{2+}, and Mn^{4+} are present in the bulk model. We could not find any other oxidation state for the TM in NMC111. This is consistent with the experimental findings, and it keeps the average formal charge of the metals equal to three.[33−35] The same was the case for all the surface slabs. However, the magnetization of the surface TM in the (104) surface was different and required further analysis. Figure 9 shows the projected density of states (PDOS) on the d orbitals of the Co ions in the slab representing the (104) surface. Figure 9b shows that, in the bulk region of the slab, the e_g orbitals $d_{x^2-y^2}$ and d_{z^2} are unoccupied. Furthermore, the magnetization is zero, indicating Co^{3+} in the low spin configuration. The t_{2g} orbitals d_{xy}, d_{xz}, and d_{yz} are in the filled state region showing occupancy in the spin up and spin down with a very similar range of energies suggesting no magnetization. This configuration is consistent with the d band splitting caused by an octahedral coordination. A schematic representation of the d orbital filling is shown in Figure 9d. The crystal field splitting energy is less than the spin pairing energy. Hence, the low spin configuration is favored. Figure 9a shows the PDOS for the Co ions in the surface layer of the slab. In this position the projection on d_{z^2} presents filled states in the spin up and empty states only in the spin down, indicating one electron in this orbital. The projection along $d_{x^2-y^2}$ indicates no electrons in this orbital. Similar to d_{z^2}, the projection along d_{xy} orbitals indicates just one electron in the spin up state. The combination of the magnetization, Bader charges, and PDOS analysis indicates Co^{3+} in an intermediate spin state. This result is in agreement with previous work[21,36] showing experimental[37] and theoretical evidence of intermediate spin of the five coordinated Co^{3+} ions at the surface of LCO.[21] Other previous work[35] has also found that changes in the coordination symmetry around Co ions change its electronic configuration, as expected. Figure 9c shows a schematic representation of the d orbital filling for the Co ions at the surface of the slab. In this case, the crystal field splitting energy is greater than the spin pairing energy in the d_{xy} orbital. This is expected for a square pyramidal coordination of the TM. Moreover, the axial oxygen is farther from the Co ion than the equatorial oxygen. The Co−O axial bond in the surface is 2.01 Å, and the equatorial bonds are 1.95 Å on average, while 1.99 Å is obtained in the bulk region. The increase in Co−O axial bond distance lowers the energy of the d_{z^2} orbital even more. This is also consistent with the magnetization of the Co ions at the surface with a value of 2.3 μB associated with t_{2g}^5 e_g^1 configuration, corresponding to an intermediate spin.

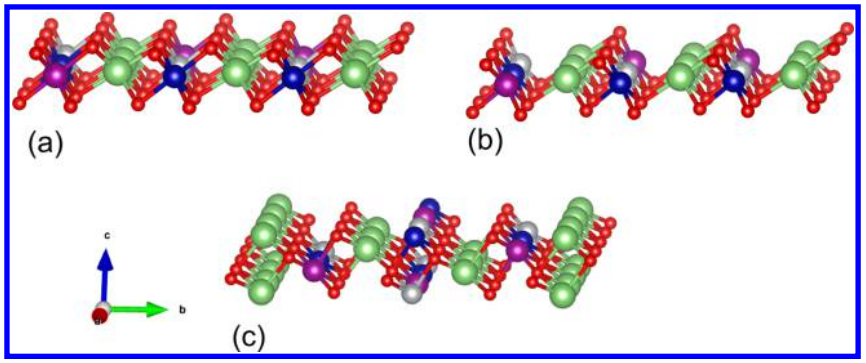

Figure 8. First three layers of the (012) surface. (a) One monolayer of oxygen coverage, which produces a surface dipole. (b) Half a monolayer of oxygen coverage, which produces a stoichiometric ratio of the elements and a nonpolar surface. (c) Schematic representation of the top three layers of the (100) surface.

DOI: 10.1021/acs.jpcc.7b00896
J. Phys. Chem. C XXXX, XXX, XXX−XXX

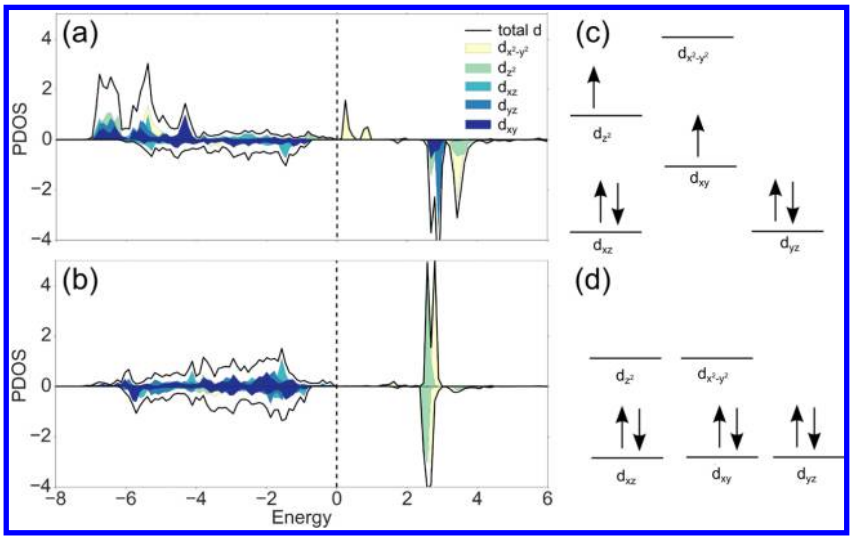

Figure 9. Co PDOS d-orbitals. (a) Co in the surface layer of the slab. (b) Co in the bulk region of the slab. (c) Surface layer Co d orbital electronic configuration scheme. (d) Bulk Co d orbital electronic configuration scheme.

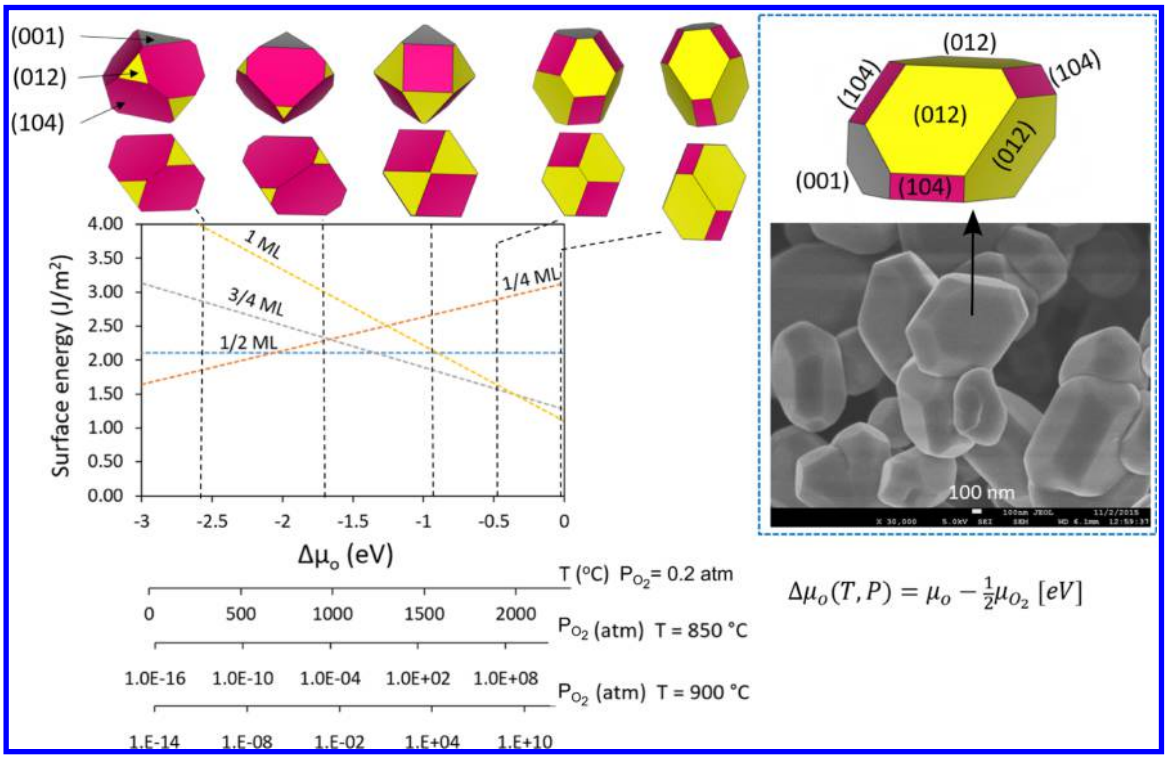

Figure 10. Surface energy of the (012) facet as a function of the oxygen chemical potential. The crystal particle shape from the Wulff construction is shown at select conditions indicated by the dotted lines. A SEM image of the synthesized particles is also shown.

These results were obtained while keeping the ions in the bulk region of the slab fixed and relaxing only the two outermost layers of the surface. When the entire slab was relaxed, a distortion of the octahedron formed by the oxygen ions around the TM was observed. The axial Co−O bond (2.21 Å) in the inner layers of the slab is greater than that in the "fixed" bulk model (1.99 Å). Also, the equatorial Co−O bonds became shorter (1.96 Å). This distortion produces Co^{3+} ions in the intermediate spin state in the bulk region of the slab, which is not expected. This suggests that thicker slabs (>9 layer) should be used or that the inner layers should be fixed to bulk values to get more reliable results. However, a thicker slab would be computationally expensive. Therefore, the bulk region was fixed to avoid this issue. Co^{3+} was also found in a high spin state at the surface caused by the large distortion (axial Co−O bond 1.98 Å) of the symmetry around the TM when all the atoms in the slab were relaxed. High spin states of Co^{3+} at LCO (104) surfaces, with square pyramidal coordination, have been reported.[38] Qian et al.[21] found that the surface energies are minimized when the surface Co^{3+} ions are in either the intermediate or high spin states. They found an energy of 0.31 J/m^2 for the (104) surface of LCO with intermediate/high spin Co^{3+} compared to 1.0 J/m^2 for a (104) surface with low spin Co^{3+}. We also found a low value (0.79 J/m^2) for the energy of the (104) surface of NMC111 when considering high/intermediate spin Co^{3+}. This seems to be consistent with the

DOI: 10.1021/acs.jpcc.7b00896
J. Phys. Chem. C XXXX, XXX, XXX−XXX

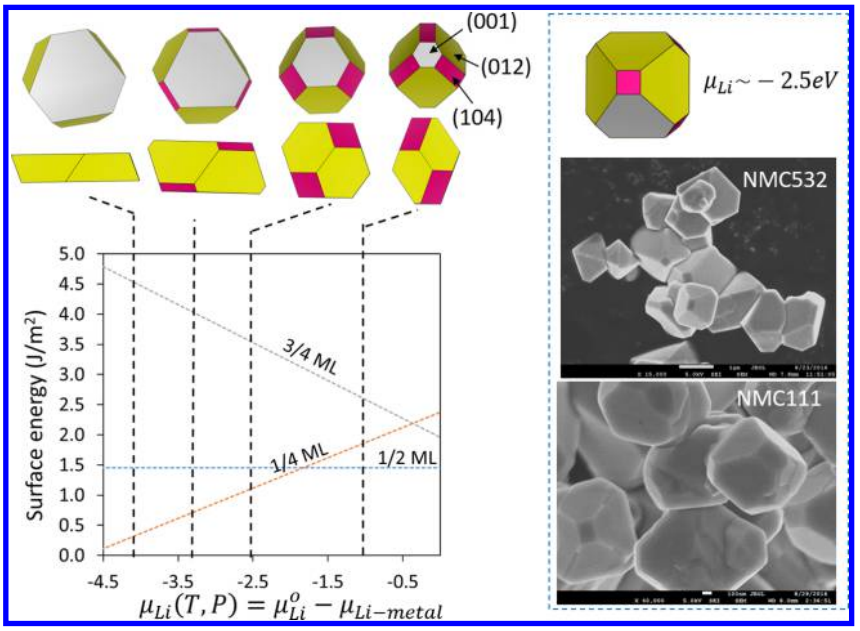

Figure 11. Surface energy of the (001) facet as a function of the Li chemical potential. The crystal particle shape from the Wulff construction is shown at select conditions indicated by the dotted lines. The inset shows a SEM image of synthesized NMC crystals for comparison with the constructed particle shape.

value found for LCO since NMC111 has a lower concentration of Co^{3+}. The rest of the TMs (Ni^{2+} and Mn^{4+}) do not present any change in spin state because they are already in high spin states at these oxidation states. The stabilization produced by Co at the surface generates a driving force for segregation to this specific facet. Previous work[10] has shown Co segregation to the $(20\bar{2})$ surface of a monoclinic cell for a layered NMC material, which is equivalent to the (104) surface using a hexagonal unit cell.

The (012) surface has also five-coordinate Co ions at the surface for the stoichiometric composition (1/2 monolayer of oxygen). However, the magnetization of the Co ions at the surface is zero. Hence, Co^{3+} at the (012) surface is present in the low spin state. The spin state is different despite having the same coordination as the ions at the (104) surface. This may be a consequence of the different distortions of the square pyramids formed at the surface. The square pyramids at the surface form an angle of about 45° with the surface leaving two of the equatorial oxygen under-coordinated compared with the oxygen in the bulk region. These two bonds are shorter (1.8 Å) than the other two equatorial bonds (2.1 Å) and the axial bond (2.02 Å). This distortion produces a different crystal field. According to our findings, this configuration does not favor an intermediate or high spin state.

3.2. Thermodynamic Analysis of the Polar Surfaces. In order to predict the equilibrium particle shape of NMC111 crystals, it is necessary to take into account the conditions of the surrounding environment. Based on the possible surface compositions, there are two types of surfaces susceptible to changes with the synthesis conditions. Namely, the (012) surface is sensitive to changes in the oxygen chemical potential and the (001) surface is susceptible to changes in the Li chemical potential. Figure 10 shows the relationship between the surface energy and the oxygen chemical potential for five different oxygen coverage values on the (012) surface. The surface with a full monolayer of oxygen is favored at high oxygen chemical potentials (oxygen-rich environment). Highly oxidizing environments would lead to more stable (012) surfaces. It can be seen in Figure 10 that for those conditions the (012) surface dominates energetically. The inset in Figure 10 shows a scanning electron microscopy (SEM) image of NMC532 crystals synthesized using $Mn(NO_3)_2{\cdot}4H_2O$, $Co(NO_3)_2{\cdot}6H_2O$, and $Ni(NO_3)_2{\cdot}6H_2O$ as TM precursors, 1.1 × $LiNO_3$ as Li source and CsCl as the flux (R = 2). The sample was obtained after heating in air at 850 °C for 8 h and then cooling at a controlled rate of 4 °C/min. In agreement with the theoretical calculation, about 70% of the exposed crystal surfaces are (012) facets. In contrast, in a less oxidizing environment, the predicted shape is dominated by the (104) surface, which is the most stable at stoichiometric conditions. The (001) surface appears in the particle at all conditions at a practically constant proportion. However, this surface is covered by 1/2 of a monolayer of lithium and hence sensitive to variations in the chemical potential of Li.

The experimental conditions are complex and hard to directly relate with the theoretical calculations. However, one can gain some insight from the temperature and oxygen partial pressure dependence. The chemical potential axis can be expressed in terms of the temperature at a given pressure or in terms of the pressure at a given temperature. Three examples are shown in Figure 10. The second axis shows that for a given pressure (0.2 atm) higher temperatures favor the formation of the (012) surface. The third and fourth axes show that higher partial pressures of oxygen also favor a higher coverage and the stabilization of the (012) surface.

The chemical potential of lithium changes with lithium content during the synthesis of the material and during cycling. Although, during cycling kinetic barriers impede changes in the particle shape. Figure 11 shows the (001) surface energy change with the chemical potential of Li at an oxygen chemical potential value of −0.1 eV. This surface becomes predominant at 1/4 of monolayer Li coverage on the surface, adopting a platelet shape. With increasing Li chemical potential, the particles adopt more polyhedral shape. Excellent agreement

DOI: 10.1021/acs.jpcc.7b00896
J. Phys. Chem. C XXXX, XXX, XXX−XXX

with experimental results was obtained under the high O and low Li chemical potential conditions. Figure 11 inset shows the SEM image of NMC532 crystals synthesized using $Mn(NO_3)_2 \cdot 4H_2O$, $Co(NO_3)_2 \cdot 6H_2O$, and $Ni(NO_3)_2 \cdot 6H_2O$ as TM precursors, Li_2CO_3 as Li source, and CsCl as the flux (R = 4). The crystals were obtained after heating in air at 900 °C for 12 h and then cooling to room temperature at 4 °C/min. The same morphology was also found on NMC111 crystals synthesized under similar conditions, as shown in the SEM image in Figure 11. As can be seen from Figures 10 and 11, an NMC composition in the range of 111 to 532 does not alter the main conclusions of particle morphology drawn from our calculations of NMC111, implying some generality. However, as the relative Ni content increases, the effect of Li/Ni exchange and/or TM segregation may play an important role. Studies along these lines are currently in progress.

3.3. Oxygen Vacancy Formation Analysis. The oxygen vacancy formation energy at the surface can be considered an indication of the surface propensity to reduction. The (104) surface has three different kinds of oxygen atoms. In the bulk, oxygen atoms occupy the vertices of the octahedron (four equatorial and two axial M−O bonds). Surface oxygen atoms in the (104) surface form the equatorial M−O bonds, while the oxygen in the second layer forms the axial M−O bond. Surface oxygen atoms are also the vertex of the inverted square pyramid formed by the cleaved surface plane. Note that surface oxygen is always coordinated to the three TM (Ni^{2+}, Mn^{4+}, Co^{3+}). However, there are three different configurations depending on the nature of the TM axially coordinated with the oxygen. In the case of the (012) surface, oxygen atoms are coordinated to two TMs in an equatorial configuration.

Table 2 shows the oxygen vacancy formation energy of each oxygen type on the (104) and (012) surfaces. The results show

Table 2. Oxygen Vacancy Formation Energy on the (104) and (012) Surfaces

surface	coordination	energy of formation of an oxygen vacancy (eV)
(104)	Co; axial	5.4
	Ni; axial	2.2
	Mn; axial	1.5
(012)	Co, Ni; equatorial	1.9
	Co, Mn; equatorial	1.1
	Mn, Ni; equatorial	0.6

that, on the (104) surface, the oxygen that is axially coordinated to Mn is the easiest to remove, followed by Ni and, finally, Co. A similar trend is observed for the (012) surface. Specifically, oxygen is more difficult to remove when it is coordinated to Co. The oxygen-vacancy defect would be primarily located on top of Mn ions. This observation could have important consequences, as under-coordinated surface Mn could constitute a possible pathway for the preferential dissolution of Mn. However, TM dissolution study requires a more complex model that takes into account the electrolyte and other magnetic and electronic effects. For instance, surface reduction can occur not only with the formation of oxygen vacancies but also as a result of a reaction with the electrolyte, such as with EC.[39]

The energy of formation of oxygen vacancies changes with the content of lithium in the material as shown in Figure 12. The process of removing an oxygen atom from the surface

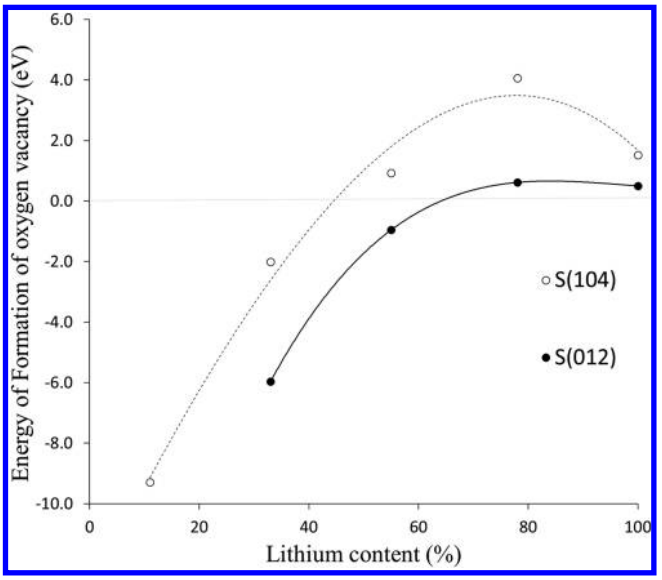

Figure 12. Energy of formation of an oxygen vacancy on the (104) and (012) surfaces of $Li(Ni_{1/3}Mn_{1/3}Co_{1/3})O_2$ as a function of Li content in the slab.

leaves two unpaired electrons in the lattice. Thus, the material is reduced upon formation of an oxygen vacancy. On the contrary, the delithiation process leads to the oxidation of the material. The lower the lithium content (high SOC, high voltage), the easier it is to reduce the surface. Indeed, for lithium contents below ~40% (60% SOC), the release of oxygen from the (104) surface becomes a spontaneous process. However, for the (012) surface this process becomes spontaneous for lithium contents below 60% (40% SOC). This is an indication of the reactivity of the surface oxygen atoms of these surfaces. Specifically, our results indicate that (012) surfaces would be more reactive toward electrolyte oxidation due to the relative ease of oxygen vacancy formation with respect to the (104) surfaces. Conversely, (104) surfaces should be more robust with respect to electrolyte interactions. This trend is also consistent with the calculated surface energies of these two surfaces where the surface energy of the (104) facet is lower than the surface energy of (012) facet (see Table 1).

4. CONCLUSIONS

Atomistic simulations based on first-principles density functional theory at the GGA+U level, as well as at the hybrid HSE06 level, were performed to investigate the stability of several low-index surfaces of $Li(Ni_{1/3}Mn_{1/3}Co_{1/3})O_2$ (NMC111) as a function of Li and O chemical potentials. The morphology and crystal shape dependence on changes in chemical potentials (oxygen and lithium) were also explored. A good agreement between the predicted particle shapes and those of single-crystal NMCs (111 and 532), synthesized under different conditions, was obtained. Valuable insights were presented into not only the effects of O and Li environments during synthesis but also into the determination of the crystal facets and surface terminations most relevant for further studies. We found that only the (104), (012), and (001) facets appear in the equilibrium shapes. The predominant surface for a highly oxidizing environment is the (012). Lower values of the Li chemical potential would produce more platelet-shaped particles. Additionally, we found evidence of intermediate spin

DOI: 10.1021/acs.jpcc.7b00896
J. Phys. Chem. C XXXX, XXX, XXX−XXX

states for the Co^{3+} ions at the surface of the (104) facet. This electronic configuration is linked with the high stability of the (104) surface. We also found evidence of preferential defect formation at sites where oxygen is coordinated to Mn. This result has possible implications for mechanistic studies on Mn-ion dissolution. Furthermore, the energy of formation of an oxygen vacancy depends on the content of lithium (SOC). The release of oxygen becomes spontaneous for delithiation levels higher than 60% for the (104) surface and 40% for the (012) surface. Based on these results, choosing synthesis conditions that favor the formation of (104) over (012) facets may enhance the electrochemical stability of NMC particles.

AUTHOR INFORMATION

Corresponding Author

*E-mail: iddir@anl.gov. Phone: 630-252-4505.

ORCID

Juan C. Garcia: 0000-0002-5911-8850

Guoying Chen: 0000-0002-3218-2609

Notes

The authors declare no competing financial interest.

ACKNOWLEDGMENTS

We are grateful to Anthony Burrell (NREL) and others in the Argonne High Energy High Voltage team, for helpful discussions. We are also grateful to Roy Benedek and Larry Curtiss for their comments on the manuscript. The authors thank Dr. Saravanan Kuppan for helping with crystal synthesis. The submitted manuscript has been created by UChicago Argonne, LLC, Operator of Argonne National Laboratory ("Argonne"). Argonne, a U.S. Department of Energy Office of Science laboratory, is operated under Contract no. DE-AC02-06CH11357. Computer time allocations at the Argonne's Laboratory Computing Resource Center is gratefully acknowledged. Funding provided by the Vehicle Technologies Program, U.S. Department of Energy, Office of Energy Efficiency and Renewable Energy.

REFERENCES

(1) Ceder, G.; Chiang, Y.-M.; Sadoway, D. R.; Aydinol, M. K.; Jang, Y.-I.; Huang, B. Identification of Cathode Materials for Lithium Batteries Guided by First-Principles Calculations. *Nature* **1998**, *392*, 694−696.

(2) Sun, Y.-K.; Myung, S.-T.; Park, B.-C.; Prakash, J.; Belharouak, I.; Amine, K. High-Energy Cathode Material for Long-Life and Safe Lithium Batteries. *Nat. Mater.* **2009**, *8*, 320−324.

(3) Zheng, J.; Gu, M.; Genc, A.; Xiao, J.; Xu, P.; Chen, X.; Zhu, Z.; Zhao, W.; Pullan, L.; Wang, C.; et al. Mitigating Voltage Fade in Cathode Materials by Improving the Atomic Level Uniformity of Elemental Distribution. *Nano Lett.* **2014**, *14*, 2628−2635.

(4) Yabuuchi, N.; Ohzuku, T. Novel Lithium Insertion Material of $LiCo_{1/3}Ni_{1/3}Mn_{1/3}O_2$ for Advanced Lithium-Ion Batteries. *J. Power Sources* **2003**, *119*−*121*, 171−174.

(5) Tarascon, J.-M.; Armand, M. Issues and Challenges Facing Rechargeable Lithium Batteries. *Nature* **2001**, *414*, 359−367.

(6) Lu, Z.; MacNeil, D. D.; Dahn, J. R. Layered $Li[Ni_XCo_{1-2X}Mn_X]O_2$ Cathode Materials for Lithium-Ion Batteries. *Electrochem. Solid-State Lett.* **2001**, *4*, A200−A203.

(7) Arroyo y de Dompablo, M. E.; Marianetti, C.; Van der Ven, A.; Ceder, G. Jahn-Teller Mediated Ordering in Layered Li_XMO_2 Compounds. *Phys. Rev. B: Condens. Matter Mater. Phys.* **2001**, *63*, 144107.

(8) Bhatt, M. D.; O'Dwyer, C. Recent Progress in Theoretical and Computational Investigations of Li-Ion Battery Materials and Electrolytes. *Phys. Chem. Chem. Phys.* **2015**, *17*, 4799−4844.

(9) Yin, S.-C.; Rho, Y.-H.; Swainson, I.; Nazar, L. F. X-ray/Neutron Diffraction and Electrochemical Studies of Lithium De/Re-Intercalation in $Li_{1-x}Co_{1/3}Ni_{1/3}Mn_{1/3}O_2$ (X = 0 → 1). *Chem. Mater.* **2006**, *18*, 1901−1910.

(10) Yan, P.; Zheng, J.; Zheng, J.; Wang, Z.; Teng, G.; Kuppan, S.; Xiao, J.; Chen, G.; Pan, F.; Zhang, J.-G.; et al. Ni and Co Segregations on Selective Surface Facets and Rational Design of Layered Lithium Transition-Metal Oxide Cathodes. *Adv. Energy Mater.* **2016**, *6*, 1502455.

(11) Gu, M.; Belharouak, I.; Genc, A.; Wang, Z.; Wang, D.; Amine, K.; Gao, F.; Zhou, G.; Thevuthasan, S.; Baer, D. R.; et al. Conflicting Roles of Nickel in Controlling Cathode Performance in Lithium Ion Batteries. *Nano Lett.* **2012**, *12*, 5186−5191.

(12) Lin, F.; Markus, I. M.; Nordlund, D.; Weng, T.-C.; Asta, M. D.; Xin, H. L.; Doeff, M. M. Surface Reconstruction and Chemical Evolution of Stoichiometric Layered Cathode Materials for Lithium-Ion Batteries. *Nat. Commun.* **2014**, *5*, 3529.

(13) Lin, F.; Nordlund, D.; Li, Y.; Quan, M. K.; Cheng, L.; Weng, T.-C.; Liu, Y.; Xin, H. L.; Doeff, M. M. Metal Segregation in Hierarchically Structured Cathode Materials for High-Energy Lithium Batteries. *Nat. Energy* **2016**, *1*, 15004.

(14) Chen, G.; Hai, B.; Shukla, A. K.; Duncan, H. Impact of Initial Li Content on Kinetics and Stabilities of Layered $Li_{1+x}(Ni_{0.33}Mn_{0.33}Co_{0.33})_{1-x}O_2$. *J. Electrochem. Soc.* **2012**, *159*, A1543−A1550.

(15) Gilbert, J. A.; Bareño, J.; Spila, T.; Trask, S. E.; Miller, D. J.; Polzin, B. J.; Jansen, A. N.; Abraham, D. P. Cycling Behavior of NCM523/Graphite Lithium-Ion Cells in the 3−4.4 V Range: Diagnostic Studies of Full Cells and Harvested Electrodes. *J. Electrochem. Soc.* **2017**, *164*, A6054−A6065.

(16) Gilbert, J. A.; Shkrob, I. A.; Abraham, D. P. Transition Metal Dissolution, Ion Migration, Electrocatalytic Reduction and Capacity Loss in Lithium-Ion Full Cells. *J. Electrochem. Soc.* **2017**, *164*, A389−A399.

(17) Shkrob, I. A.; Kropf, A. J.; Marin, T. W.; Li, Y.; Poluektov, O. G.; Niklas, J.; Abraham, D. P. Manganese in Graphite Anode and Capacity Fade in Li Ion Batteries. *J. Phys. Chem. C* **2014**, *118*, 24335−24348.

(18) Chen, K.; Xue, D. Materials Chemistry toward Electrochemical Energy Storage. *J. Mater. Chem. A* **2016**, *4*, 7522−7537.

(19) Kramer, D.; Ceder, G. Tailoring the Morphology of $LiCoO_2$: A First Principles Study. *Chem. Mater.* **2009**, *21*, 3799−3809.

(20) Okubo, M.; Hosono, E.; Kim, J.; Enomoto, M.; Kojima, N.; Kudo, T.; Zhou, H.; Honma, I. Nanosize Effect on High-Rate Li-Ion Intercalation in $LiCoO_2$ Electrode. *J. Am. Chem. Soc.* **2007**, *129*, 7444−7452.

(21) Qian, D.; Hinuma, Y.; Chen, H.; Du, L.-S.; Carroll, K. J.; Ceder, G.; Grey, C. P.; Meng, Y. S. Electronic Spin Transition in Nanosize Stoichiometric Lithium Cobalt Oxide. *J. Am. Chem. Soc.* **2012**, *134*, 6096−6099.

(22) Kim, Y.; Lee, H.; Kang, S. First-Principles and Experimental Investigation of the Morphology of Layer-Structured $LiNiO_2$ and $LiCoO_2$. *J. Mater. Chem.* **2012**, *22*, 12874−12881.

(23) Cahn, J. W.; Carter, W. C. Crystal Shapes and Phase Equilibria: A Common Mathematical Basis. *Metall. Mater. Trans. A* **1996**, *27*, 1431−1440.

(24) Kresse, G.; Furthmüller, J. Efficiency of Ab-Initio Total Energy Calculations for Metals and Semiconductors Using a Plane-Wave Basis Set. *Comput. Mater. Sci.* **1996**, *6*, 15−50.

(25) Kresse, G.; Hafner, J. Ab Initio Molecular Dynamics for Liquid Metals. *Phys. Rev. B: Condens. Matter Mater. Phys.* **1993**, *47*, 558−561.

(26) Perdew, J. P.; Burke, K.; Ernzerhof, M. Generalized Gradient Approximation Made Simple. *Phys. Rev. Lett.* **1996**, *77*, 3865−3868.

(27) Blöchl, P. E. Projector Augmented-Wave Method. *Phys. Rev. B: Condens. Matter Mater. Phys.* **1994**, *50*, 17953−17979.

DOI: 10.1021/acs.jpcc.7b00896
J. Phys. Chem. C XXXX, XXX, XXX−XXX

(28) Iddir, H.; Benedek, R. First-Principles Analysis of Phase Stability in Layered−Layered Composite Cathodes for Lithium-Ion Batteries. *Chem. Mater.* **2014**, *26*, 2407−2413.
(29) Heyd, J.; Scuseria, G. E.; Ernzerhof, M. Hybrid Functionals Based on a Screened Coulomb Potential. *J. Chem. Phys.* **2003**, *118*, 8207−8215.
(30) Cahill, L. S.; Yin, S.-C.; Samoson, A.; Heinmaa, I.; Nazar, L. F.; Goward, G. R. 6Li NMR Studies of Cation Disorder and Transition Metal Ordering in $Li[Ni_{1/3}Mn_{1/3}Co_{1/3}]O_2$ Using Ultrafast Magic Angle Spinning. *Chem. Mater.* **2005**, *17*, 6560−6566.
(31) Tasker, P. W. The Stability of Ionic Crystal Surfaces. *J. Phys. C: Solid State Phys.* **1979**, *12*, 4977.
(32) Benedek, R.; Thackeray, M. M. Simulation of the Surface Structure of Lithium Manganese Oxide Spinel. *Phys. Rev. B: Condens. Matter Mater. Phys.* **2011**, *83*, 195439.
(33) Nayak, P. K.; Grinblat, J.; Levi, M.; Markovsky, B.; Aurbach, D. Structural and Electrochemical Evidence of Layered to Spinel Phase Transformation of Li and Mn Rich Layered Cathode Materials of the Formulae $xLi[Li_{1/3}Mn_{2/3}]O_2(1\text{-}x)LiMn_{1/3}Ni_{1/3}Co_{1/3}O_2$ (X = 0.2, 0.4, 0.6) upon Cycling. *J. Electrochem. Soc.* **2014**, *161*, A1534−A1547.
(34) Dixit, M.; Kosa, M.; Lavi, O. S.; Markovsky, B.; Aurbach, D.; Major, D. T. Thermodynamic and Kinetic Studies of LiNi0.5Co0.2Mn0.3O2 as a Positive Electrode Material for Li-Ion Batteries Using First Principles. *Phys. Chem. Chem. Phys.* **2016**, *18*, 6799−6812.
(35) Lim, J.-M.; Kim, D.; Park, M.-S.; Cho, M.; Cho, K. Underlying Mechanisms of the Synergistic Role of Li_2MnO_3 and $LiNi_{1/3}Co_{1/3}Mn_{1/3}O_2$ in High-Mn, Li-Rich Oxides. *Phys. Chem. Chem. Phys.* **2016**, *18*, 11411−11421.
(36) Carlier, D.; Cheng, J.-H.; Pan, C.-J.; Ménétrier, M.; Delmas, C.; Hwang, B.-J. DFT+U Calculations and XAS Study: Further Confirmation of the Presence of CoO_5 Square-Based Pyramids with IS-Co^{3+} in Li-Overstoichiometric $LiCoO_2$. *J. Phys. Chem. C* **2013**, *117*, 26493−26500.
(37) Maram, P. S.; Costa, G. C. C.; Navrotsky, A. Experimental Confirmation of Low Surface Energy in $LiCoO_2$ and Implications for Lithium Battery Electrodes. *Angew. Chem., Int. Ed.* **2013**, *52*, 12139−12142.
(38) Vallverdu, G.; Minvielle, M.; Andreu, N.; Gonbeau, D.; Baraille, I. First Principle Study of the Surface Reactivity of Layered Lithium Oxides $LiMO_2$ (M = Ni, Mn, Co). *Surf. Sci.* **2016**, *649*, 46−55.
(39) Leung, K. First-Principles Modeling of the Initial Stages of Organic Solvent Decomposition on $Li_xMn_2O_4(100)$ Surfaces. *J. Phys. Chem. C* **2012**, *116*, 9852−9861.

DOI: 10.1021/acs.jpcc.7b00896
J. Phys. Chem. C XXXX, XXX, XXX−XXX